# Polysulfide Chalcogels with Ion-Exchange Properties and Highly Efficient Mercury Vapor Sorption

Youngtak Oh, Collin D. Morris, and Mercouri G. Kanatzidis*

Department of Chemistry, Northwestern University, 2145 Sheridan Road, Evanston, Illinois 60208, United States

S Supporting Information

ABSTRACT: We report the synthesis of metal–chalcogenide aerogels from Pt^{2+} and polysulfide clusters ($[S_x]^{2-}$, $x = 3-6$). The cross-linking reaction of these ionic building blocks in formamide solution results in spontaneous gelation and eventually forms a monolithic dark brown gel. The wet gel is transformed into a highly porous aerogel by solvent exchanging and subsequent supercritical drying with CO_2. The resulting platinum polysulfide aerogels possess a highly porous and amorphous structure with an intact polysulfide backbone. These chalcogels feature an anionic network that is charged balanced with potassium cations, and hosts highly accessible S–S bonding sites, which allows for reversible cation exchange and mercury vapor capture that is superior to any known material.
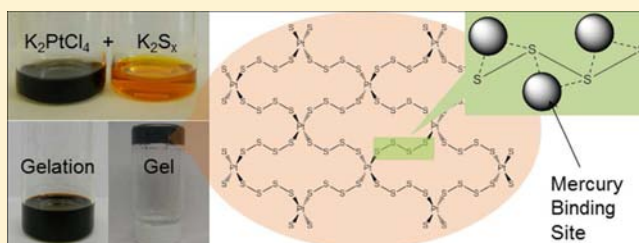
INTRODUCTION

Aerogels are three-dimensional random networks with highly accessible nanoscale pores and very low densities. Metal–oxide aerogels are the dominant examples in this class and useful in applications such as catalysis, thermal insulation, adsorbents, and sensors.[1] A novel kind of emerging aerogel features metal–chalcogenide networks instead of metal oxide.[2−5] The metal–chalcogenide aerogels, dubbed chalcogels, exhibit a unique combination of porous structures with visible and infrared light absorption, surface polarizability, and chemical selectivity. These chalcogels show promise in areas such as solar-fuel catalysis,[6] photoluminescence,[7] selective gas separation,[8] catalysis,[9] and heavy metal aqueous waste remediation.[10]

There are three main methods to producing metal–chalcogenide aerogels: thiolysis,[11−13] nanoparticle oxidation and condensation,[2,3,7,14,15] and sol–gel metathesis.[6,8−10,16] Among these, the metathesis route shows wide applicability in the synthesis of chalcogels because of the simplicity of the reaction and diversity in the choice of building blocks. Using this approach, our group has demonstrated the synthesis of chalcogenide aerogels using primary building blocks such as tetrahedral clusters ($[MQ_4]^{4-}$ and $[M_2Q_6]^{4-}$, M = Mo, Sn, Ge/Q = S, Se),[9,10,16] and adamantine clusters ($[M_4Q_{10}]^{4-}$, M = Sn, Ge/Q = S, Se),[16] Figure 1A. These versatile choices of building blocks incorporate chemical diversity into enormously porous structures to produce materials with broad functionalities that can surpass those of conventional metal–oxide aerogels.

One such outstanding functionality of chalcogels is selective adsorption of ions and molecules. Platinum chalcogels[16] and zinc tin sulfide chalcogels (e.g., ZTS-cg1)[10] are representative examples that illustrate how these soft Lewis basic surfaces are effective in selectively removing heavy metal ions (e.g., Hg^{2+}) from aqueous solutions. To date, no chalcogels have been
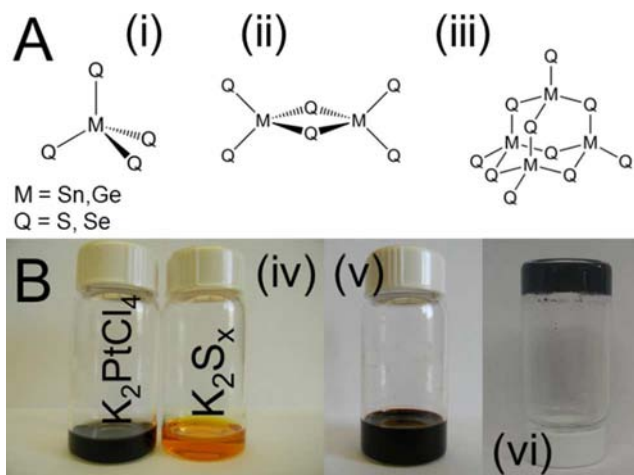

Figure 1. (A) Building blocks of chalcogel for metathesis route: (i) tetrahedral cluster, (ii) dimeric tetrahedral cluster, and (iii) adamantane cluster. (B) Photographic illustration of metathesis process: (iv) precursor solutions containing inorganic building blocks, (v) mixture of precursor solution undergoing gelation (cross-linking reaction), and (vi) completed metathesis reaction yielding monolithic wet gel.

tested for the remediation of gas-phase pollutants such as elemental mercury. As a major toxic pollutant from flue gases (coal combustion exhaust gas), elemental mercury (Hg^0) poses a great challenge to its removal because conventional air pollution control techniques such as fabric filtering (FF), electrostatic precipitation (ESP), and flue-gas desulfurization

(FGD) are not effective.[17,18] To control elemental mercury vapor from flue gas, highly adsorptive materials such as activated carbon have been employed, but display low Hg capture capacity at elevated temperatures, and suffer from interference of adsorption by other flue gas chemicals such as SO_3. Functionalization of activated carbon with functional groups such as chloride,[19] iodide,[20] and sulfide[21] shows improvements in mercury capture efficiency,[20] but contamination of reusable combustion products (fly ash) by activated carbon remains problematic. In contrast, sulfur-functionalized noncarbon materials such as Co-doped silica,[22] Co-doped iron nanoparticles,[23] porous silica,[24] and silica–titania nanocomposites[25] possess high mercury capture capacities without the problems of carbon-based materials. These studies showed higher mercury capture capacity on samples with more sulfur content; thus it would be interesting in this regard to study the Hg absorption properties of purely sulfidic porous networks such as those of chalcogels.

In this study, we present the synthesis of a novel class of chalcogels with high surface areas featuring different polysulfides and platinum ($K–Pt–S_x$). These porous metal–chalcogenide compounds have ditopic linear polysulfide ligands (i.e., S_x^{2-}, $x = 3, 4, 5, 6$). The framework motif is similar to the crystalline compounds of $(Ph_4P)[M(Se_6)_2]$ (M = Ga, In, Tl), which are an exceptional example of an open framework with a polyselenide backbone; however, they lack accessible pores.[26] We show that the networks in these new $K–Pt–S_x$ chalcogels are anionically charged and potassium cations balance the charge. Therefore, these materials possess dual functionality: (a) ion-exchange properties and (b) S–S bonds capable of undergoing reductive cleavage with, for example, Hg°. We demonstrate here that these materials are the first examples of chalcogels featuring both ion-exchange properties and elemental mercury capture abilities. We characterize the chemical and physical identity of the polysulfide chalcogels and show the pivotal role of the S–S bridging sites of the polysulfide ligands in mercury capture experiments. Finally, we show the ion-exchange functionality of our platinum polysulfide chalcogels for aqueous environmental waste remediation.

■ RESULT AND DISCUSSION

The reaction between Pt^{2+} and S_x^{2-} precursors at room temperature leads to a polymeric three-dimensional inorganic framework. A formamide solution containing K_2S_x ($x = 3–6$) was slowly added to a formamide solution with an equivalent molar amount of K_2PtCl_4 resulting in a spontaneous cross-linking reaction between Pt^{2+} and S_x^{2-} units. Upon mixing of the two precursor solutions, a clear deep red colloidal solution appeared. As the reaction progressed, the viscosity of the solution increased, and eventually formed a monolithic dark brown gel after 2 d. To process this wet gel into an aerogel, a solvent exchange was conducted with $EtOH:H_2O$ (4:1) solution for 5 d, followed by EtOH for 5 d, and subsequently supercritically dried with CO_2. These procedures were necessary to extract liquid components out of gel structure without destroying the porous network. With this treatment, the monolithic wet gel was transformed into a fluffy dark brown aerogel retaining the shape and volume of the original wet-gel.[6,9,10,16] A schematic of a proposed structure adopted by these chalcogels is shown in Figure 2. These schematic model of the $K–Pt–S_x$ chalcogel structure was inspired by the previously reported open framework crystal structures of $K_2Pd(Se_x)_2$, and $(Ph_4P)In(Se_6)_2$ featuring polyselenide
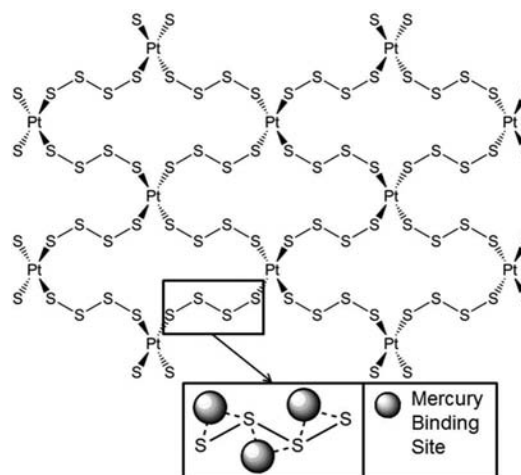

Figure 2. A proposed structure and potential mercury binding chemisorption sites of tetra-polysulfide chalcogel.

$[Se_x]^{2-}$ ligands.[26,27] These polychalcogenide ligand structures are consistent with the experimental results presented here such as gas and Hg absorption and ion-exchange capability of the chalcogels (see below).

Scanning electron microscope (SEM) images indicate a sponge-like character containing randomly oriented pores throughout the micrometer-sized specimens shown in Figure 3A and 1S (Supporting Information). To confirm the presence
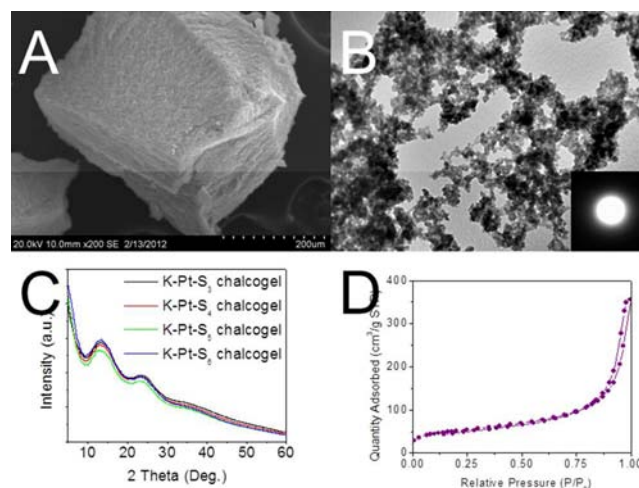

Figure 3. (A) Scanning electron microscopy (SEM) image of $K–Pt–S_x$ chalcogel. (B) Transmission electron microscope (TEM) image of $K–Pt–S_x$ chalcogel. (C) Powder X-ray diffraction pattern of polysulfide chalcogels. (D) Typical nitrogen adsorption isotherm of $K–Pt–S_x$ chalcogels.

of incorporated inorganic building blocks (Pt^{2+}, S_x^{2-}) and to estimate the relative atomic composition of each element, we analyzed the series of chalcogels formed from different polysulfide chains (S_3^{2-}, S_4^{2-}, S_5^{2-}, S_6^{2-}) with energy dispersive X-ray spectroscopy (EDS). On the basis of EDS analysis, it was confirmed that not only are platinum and the polysulfide species present, but also potassium was incorporated as part of the chalcogel. The EDS results from several different samples showed the presence of potassium in all platinum polysulfide chalcogels. This is similar to the cobalt polysulfide chalcogels reported previously.[28] The average K/Pt/S ratio of each

chalcogel was 0.37/0.81/3 for the trisulfide (S_3^{2-}), 0.38/0.84/4 for the tetrasulfide (S_4^{2-}), 0.36/0.87/5 for pentasulfide (S_5^{2-}), and 0.30/0.87/6 for the hexasulfide (S_6^{2-}).

The K–Pt–S_x chalcogels possess excellent ion-exchange properties associated with the potassium sites. When the K–Pt–S_3 chalcogel was placed in 3 mM CsCl aqueous solution, we observed complete exchange of potassium ions with cesium ions as shown in Figure 2S. Cs^+-exchanged polysulfide chalcogels were examined by EDS analysis and showed the absence of any detectable K^+. The reverse ion-exchange reaction was also possible when the Cs^+-exchanged chalcogels were submerged with a 5 mM solution of aqueous KCl. The reverse-exchange yielded the complete replacement of Cs^+ with K^+. During the ion-exchange process, the polysulfide chalcogels retained their frameworks as shown from SEM images.

Transmission electron microscope (TEM) images of the polysulfide chalcogels revealed their nanoscale porous nature as shown in Figure 3B and Figure 3S. Because of the absence of structural directing agents during synthesis, the porous structures of these chalcogels showed no regularities in shape, size, or orientation. Electron diffraction of all samples showed only diffuse scattering indicating a random aperiodic structure. As shown in Figure 3C, this result is in agreement with the powder X-ray diffraction patterns of the K–Pt–S_x chalcogels, which show broad diffuse peaks and the absence of any crystalline phase.

On the basis of the nitrogen adsorption isotherm and Brunauer–Emmett–Teller (BET) model, these supercritically dried chalcogels possess high surface areas (74–230 m^2/g), large pore volumes (0.29–0.52 cm^3/g), and 9–15 nm average pore diameters, Table 1 and Figure 3D. These chalcogels show

Table 1. Nitrogen Porosimetry Results of Potassium Platinum Polysulfide Chalcogels (K–Pt–S_x)[a]

| chalcogel	elemental comp. (EDS)[b]	S_{BET}[c] [m^2/g]	avg. pore volume [cm^3/g]	avg. pore diameter [nm]
K–Pt–S_3	$K_{0.37}Pt_{0.81}S_3$	115–230	0.38–0.47	8–13
K–Pt–S_4	$K_{0.38}Pt_{0.84}S_4$	183–200	0.42–0.52	8–14
K–Pt–S_5	$K_{0.36}Pt_{0.87}S_5$	74–171	0.29–0.48	10–22
K–Pt–S_6	$K_{0.30}Pt_{0.87}S_6$	128–195	0.37–0.48	9–14

[a]Three different samples of each chalcogel were used to evaluate these results. [b]Composition normalized per one polysulfide chain. [c]Brunauer–Emmett–Teller (BET) surface area.

minor adsorption at low relative pressures (0 < P/P_o < 0.5), indicating that only a small fraction of the adsorption occurs in micropores ($d \leq 2$ nm). The majority of the adsorption occurs at higher relative pressures (P/P_o > 0.5) where meso- (2 < d < 50 nm) and macropores (d > 50 nm) are the main contributors.[29] At relative pressures close to the saturation

point (P/P_o > 0.8), a small hysteresis was observed for each chalcogel. This adsorption−desorption hysteresis loop (ADHL) is indicative of a percolation effect seen in disordered porous structures with large pores (d > 50 nm).[30] A gel sample dried under ambient nitrogen conditions (called a xerogel) showed very low surface area (~5 m^2/g), indicating the importance of supercritical point drying to preserve the porosities of the chalcogels.

Raman spectra of these chalcogels are consistent with the presence of S−S vibrations of polysulfide ligands, shown in Figure 4S. All chalcogels exhibited broad shifts in the region between 430 and 500 cm^{-1}. These broad peaks correspond to a number of symmetric and asymmetric stretching modes of S−S bonds in the polysulfide ligands.[31] Broadening of these bands is consistent with the amorphous nature of chalcogels, and similar broadening was observed in other glassy transition metal−polysulfide compounds.[31−33] Prominent shifts of K–Pt–S_6 chalcogel from 300 to 400 cm^{-1} match with S−S stretching peak of polycrystalline K_2S_6 indicating the K_2S_6 inclusion in the gel matrix. Infrared spectra of these chalcogels show a similar broadening of the peaks, Figure 5S. The broad absorption band between 400 and 500 cm^{-1} corresponds to the S−S stretching mode, whereas that between 300 and 400 cm^{-1} most likely arises from the presence of various platinum polysulfide stretching modes converged into one broad band.[34] The absorption at 500−520 cm^{-1} is in the region of S−Pt−S stretching modes from other platinum sulfide compounds.[35]

The K–Pt–S_x chalcogels were analyzed by thermal gravimetric analysis (TGA) to investigate weight changes caused by an increase in temperature. Under both nitrogen and air, the K–Pt–S_x chalcogels did not show any weight loss up to 200 °C, shown in Figure 6S. These results suggest that the chalcogels do not decompose at temperatures relevant to those of flue gas emission (140 °C). TGA analysis and other characterization results prompted us to test for possible Hg vapor capture. Each S−S bonding site in the chalcogel structure will be readily accessible to incoming Hg atoms and is expected to be potential mercury vapor chemisorption sites according to the equation:

$$-S - S - S - + 2Hg \rightarrow - S - Hg - S - Hg - S-$$
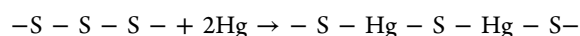
In addition to chemisorption, there is also the possibility of physisorption of Hg on the surfaces of the chalcogel. The K–Pt–S_x chalcogels were tested for mercury vapor capture in a closed vial setup. An amount of ~20 mg of each chalcogel was placed in a glass vial containing ~200 mg of elemental mercury, and the vial was kept in a heated sand bath (~140 °C) for 24 h. The chalcogel was supported above the Hg^o by conical-shaped filter paper to avoid a direct contact with elemental mercury. A scheme of the experimental set up is shown in Figure 7S.

The glass vial was cooled to room temperature, and the polysulfide chalcogel was retrieved for further analysis. To

Table 2. Mercury Vapor Capture Results for K–Pt–S_x Chalcogels[a]

Chalcogel	temp [$C°$]	adsorption capacity (ICP) [$\mu g/g$][b]	adsorption capacity (EDS) [$\mu g/g$]	theoretical chemisorption capacity[c] [$\mu g/g$]	atomic ratio of Hg-laden chalcogels (EDS)
K–Pt–S_3	140	$(1.56–3.00) \times 10^6$	$(0.81–1.01) \times 10^6$	1.47×10^6	$Hg_{1.4}K_{0.21}Pt_{0.86}S_3$
K–Pt–S_4	140	$(0.63–4.29) \times 10^6$	$(0.76–1.65) \times 10^6$	1.90×10^6	$Hg_{2.6}K_{0.27}Pt_{0.89}S_4$
K–Pt–S_5	140	$(3.20–5.45) \times 10^6$	$(0.49–1.79) \times 10^6$	2.31×10^6	$Hg_{3.1}K_{0.29}Pt_{0.82}S_5$
K–Pt–S_6	140	$(0.43–3.8) \times 10^6$	$(1.62–2.05) \times 10^6$	2.70×10^6	$Hg_{3.8}K_{0.26}Pt_{0.86}S_6$

[a]Three samples of each chalcogel were used to evaluate these results. [b]Micrograms of mercury captured per gram of adsorbent (chalcogel) used. [c]Based on the assumption that each S−S bond captures one mercury atom.

evaluate the total amount of Hg captured by either chemisorption or physisorption, we quantified the amount of mercury captured by each polysulfide chalcogel with two different methods. First, the relative elemental ratio of Hg-laden polysulfide chalcogels was used to calculate the amount of mercury bound to the surface of S–S bonding sites. In the second method, a diluted aqueous solution containing dissolved chalcogel was analyzed by ICP to quantify the total amount of mercury bound to each chalcogel.

The relative atomic ratios of the polysulfide chalcogels based on EDS analysis are $Hg_{1.4}K_{0.21}Pt_{0.86}S_3$, $Hg_{2.6}K_{0.27}Pt_{0.89}S_4$, $Hg_{3.1}K_{0.29}Pt_{0.82}S_5$, and $Hg_{3.8}K_{0.26}Pt_{0.83}S_6$ for trisulfide, tetrasulfide, pentasulfide, and hexasulfide chalcogels, respectively, Figure 8S and Table 2. This corresponds to mercury adsorption capacities of 1.01×10^6, 1.65×10^6, 1.79×10^6, and 2.05×10^6 $\mu g/g$ for the $K–Pt–S_3$, $K–Pt–S_4$, $K–Pt–S_5$, and $K–Pt–S_6$ chalcogels, respectively, which accounts for 68–86% of the theoretical chemisorption capacity; the theoretical Hg capacity for each chalcogel was calculated on the basis of the assumption that each S–S bridging site in the polysulfide ligand binds one mercury atom. All mercury-laden chalcogels showed diffraction peaks that suggest the development of crystalline HgS in the chalcogels during the Hg capturing process, Figure 9S. However, many parts of Hg-laden chalcogels retained their spongy appearance in SEM images, which suggests that major frameworks of chalcogels remained intact after the mercury capture. EDS analysis gave an underestimated amount of Hg in the chalcogels because the high e-beam absorption by Hg did not allow proper sampling of the bulk. In contrast, ICP provided a more reliable estimate via complete dissolution of the samples.

ICP evaluation showed higher mercury adsorption capacity of the $K–Pt–S_3$, $K–Pt–S_4$, $K–Pt–S_5$, and $K–Pt–S_6$ chalcogels $((1.56–3.00) \times 10^6$, $(0.63–4.29) \times 10^6$, $(3.25–5.45) \times 10^6$, and $(0.43–3.80) \times 10^6$ $\mu g/g$, respectively). The equilibrium adsorption capacity values of the polysulfide chalcogels are higher than those of any commercially used or academically studied material, including sulfur impregnated coal,[21] phenolic polymers,[21] sulfur functionalized copper doped Fe nanoparticles,[23] and sulfur functionalized porous silica,[22] Table 3.

Table 3. Mercury Vapor Adsorption Capacity of Various Absorbent Materials

	surface area [m²/g]	temp [C°]	adsorption capacity [μg/g]
$K–Pt–S_x$ CG	74–230	140	$(0.43–5.45) \times 10^5$
K_2S_3	N/A	140	N/A
ZTS-cg[a]	503–520	140	2.94×10^4
PILOT5-S40[b]	160	140	1.44×10^3
ACF-20-S40[c]	94	140	3.26×10^3
Fe–Cu–S[d]	29.6	140	$(0.17–2.73) \times 10^3$
Si-1[e]	391.3	140	1.98×10^4

[a]Zinc tin sulfide $(Zn^{2+}–[SnS_4]^{4-})$ chalcogel. [b]Sulfur impregnated coal.[21] [c]Phenolic polymer.[21] [d]Sulfur-functionalized copper-doped Fe nanoparticle.[23] [e]Copper-doped sulfur functionalized porous silica.[22]

Because our experimental setting of mercury vapor capture may be very different from the ones used to measure the value reported in the literature, the direct comparison of adsorption capacity should be made with caution. However, these high values of platinum chalcogels do confirm the mercury vapor capture functionality of polysulfide ligands. The highest

adsorption capacity of each chalcogel $((3.0–5.45) \times 10^6$ $\mu g/g)$, evaluated from ICP analysis, exceeded the theoretical estimation of full chemisorption capacity $((1.47–2.70) \times 10^6$ $\mu g/g)$. This result demonstrates that these chalcogels are highly capable of adsorbing additional mercury vapor even after all of the chemisorption sites of the polysulfide surface are occupied. Unlike the case of activated carbon, where a rise in temperature lowers the adsorption capacity, none of the polysulfide chalcogels showed any indication that increasing temperature interferes with the adsorption process. On the basis of these results, both chemisorption and physisorption contribute to mercury vapor capture; chemisorption increases as more S–S bonds (longer polysulfide chains) are available, whereas physisorption is increased as larger surface area and more porosities are available.

To better understand the effect of chalcogel surface area on Hg adsorption and further confirm that the presence of polysulfide ligands is indeed important in the Hg adsorption capacity of the $K–Pt–S_x$ chalcogels, we ran Hg capture experiments using two control groups for comparison: the first group was a crystalline compound with available S–S bonds, that is, low surface area K_2S_3, and the second group was a zinc tin sulfide chalcogel (ZTS-cg1, 503–520 m^2/g),[10] which is a very high surface area material lacking polysulfide functionality. In these experiments, the K_2S_3 sample did not show any Hg capture as determined by EDS analysis. In contrast, the ZTS-cg sample did show high adsorption capacity $((0.29–1.21) \times 10^5$ $\mu g/g)$, which is more than an order of magnitude higher than previously reported materials. However, the mercury capture efficiency of ZTS-cg was still lower relative to the $K–Pt–S_x$ chalcogels. The results from these two control groups indicate that both the rich polysulfide sites and the highly accessible porous structure of $K–Pt–S_x$ chalcogels contribute to the record high mercury adsorption efficiency.

■ CONCLUSION

New network assemblies composed of Pt^{2+} and S_x^{2-} form monolithic inorganic gels incorporating K^+. These monoliths were successfully transformed into highly porous polysulfide aerogels upon solvent exchange and supercritical drying. The $K–Pt–S_x$ chalcogels are thermally stable up to 200 °C under nitrogen or air, demonstrating the durability of these materials at flue gas temperatures. The polysulfide chalcogels show high Hg vapor adsorption capacity, which confirms that both polysulfide functionality and accessible pores contribute to the mercury vapor capture efficiency. Furthermore, the potassium sites of the polysulfide chalcogels exhibit reversible ion-exchange functionality. These preliminary results open up the possibility of using ion-exchangeable chalcogel materials for water remediation to remove toxic metal ions via replacement of potassium ions. Future studies aimed at evaluating Hg adsorption of these chalcogels in realistic flue gas conditions, in which O_2, CO_2, and SO_2 are continuously flowing with mercury vapor, are needed. Of course, the K–Pt–S chalcogels can only be regarded to be model systems given the presence of platinum. These results, however, clearly point to the high potential of chalcogels in environmental application, and we anticipate usage of other widely available linking metals such as Ni^{2+}, Zn^{2+}, Fe^{2+}, Cu^{2+}, $Sn^{2+/4+}$, etc., as alternatives to platinum that will create practical low cost materials for Hg vapor capture using the paradigm shown here.

■ ASSOCIATED CONTENT

ⓈSupporting Information

Experimental and characterization details. This material is available free of charge via the Internet at http://pubs.acs.org.

■ AUTHOR INFORMATION

Corresponding Author

m-kanatzidis@northwestern.edu

Notes

The authors declare no competing financial interest.

■ ACKNOWLEDGMENTS

■ REFERENCES

(1) Husing, N.; Schubert, U. *Angew. Chem., Int. Ed.* **1998**, *37*, 23.

(2) Arachchige, I. U.; Brock, S. L. *Acc. Chem. Res.* **2007**, *40*, 801.

(3) Arachchige, I. U.; Mohanan, J. L.; Brock, S. L. *Chem. Mater.* **2005**, *17*, 6644.

(4) Brock, S. L.; Arachchige, I. U.; Kalebaila, K. K. *Comments Inorg. Chem.* **2006**, *27*, 103.

(5) Mohanan, J. L.; Brock, S. L. *J. Non-Cryst. Solids* **2004**, *350*, 1.

(6) Yuhas, B. D.; Smeigh, A. L.; Samuel, A. P. S.; Shim, Y.; Bag, S.; Douvalis, A. P.; Wasielewski, M. R.; Kanatzidis, M. G. *J. Am. Chem. Soc.* **2011**, *133*, 7252.

(7) Arachchige, I. U.; Brock, S. L. *J. Am. Chem. Soc.* **2007**, *129*, 1840.

(8) Bag, S.; Kanatzidis, M. G. *J. Am. Chem. Soc.* **2010**, *132*, 14951.

(9) Bag, S.; Gaudette, A. F.; Bussell, M. E.; Kanatzidis, M. G. *Nat. Chem.* **2009**, *1*, 217.

(10) Oh, Y.; Bag, S.; Malliakas, C. D.; Kanatzidis, M. G. *Chem. Mater.* **2011**, *23*, 2447.

(11) Stanic, V.; Pierre, A. C.; Etsell, T. H.; Mikula, R. J. *J. Non-Cryst. Solids* **1997**, *220*, 58.

(12) Stanic, V.; Pierre, A. C.; Etsell, T. H.; Mikula, R. J. *J. Phys. Chem. A* **2001**, *105*, 6136.

(13) Stanic, V.; Etsell, T. H.; Pierre, A. C.; Mikula, R. J. *Mater. Lett.* **1997**, *31*, 35.

(14) Gacoin, T.; Lahlil, K.; Larregaray, P.; Boilot, J. P. *J. Phys. Chem. B* **2001**, *105*, 10228.

(15) Gacoin, T.; Malier, L.; Boilot, J. P. *Chem. Mater.* **1997**, *9*, 1502.

(16) Bag, S.; Trikalitis, P. N.; Chupas, P. J.; Armatas, G. S.; Kanatzidis, M. G. *Science* **2007**, *317*, 490.

(17) Chu, P.; Porcella, D. B. *Water, Air, Soil Pollut.* **1995**, *80*, 135.

(18) Meij, R. *Water, Air, Soil Pollut.* **1991**, *56*, 21.

(19) Ghorishi, S. B.; Keeney, R. M.; Serre, S. D.; Gullett, B. K.; Jozewicz, W. S. *Environ. Sci. Technol.* **2002**, *36*, 4454.

(20) Huggins, F. E.; Huffman, G. P.; Dunham, G. E.; Senior, C. L. *Energy Fuels* **1999**, *13*, 114.

(21) Hsi, H. C.; Rood, M. J.; Rostam-Abadi, M.; Chen, S. G.; Chang, R. *J. Environ. Eng. Div. (Am. Soc. Civ. Eng.)* **2002**, *128*, 1080.

(22) Meyer, D. E.; Meeks, N.; Sikdar, S.; Hutson, N. D.; Hua, D.; Bhattacharyya, D. *Energy Fuels* **2008**, *22*, 2290.

(23) Meyer, D. E.; Sikdar, S. K.; Hutson, N. D.; Bhattacharyya, D. *Energy Fuels* **2007**, *21*, 2688.

(24) Meeks, N. D.; Rankin, S.; Bhattacharyya, D. *Ind. Eng. Chem. Res.* **2010**, *49*, 4687.

(25) Pitoniak, E.; Wu, C. Y.; Mazyck, D. W.; Powers, K. W.; Sigmund, W. *Environ. Sci. Technol.* **2005**, *39*, 1269.

(26) (a) Dhingra, S.; Kanatzidis, M. G. *Science* **1992**, *258*, 1769. (b) Huang, S. P.; Kanatzidis, M. G. *Inorg. Chem.* **1991**, *30*, 1455.

(c) Park, Y. B.; Kanatzidis, M. G. *Angew. Chem., Int. Ed. Engl.* **1990**, *29*, 914.

(27) Li, J.; Chen, Z.; Wang, R. J.; Proserpio, D. M. *Coord. Chem. Rev.* **1999**, *192*, 707.

(28) (a) Shafaei-Fallah, M.; He, J.; Rothenberger, A.; Kanatzidis, M. G. *J. Am. Chem. Soc.* **2011**, *133*, 1200. (b) Shafaei-Fallah, M.; Rothenberger, A.; Katsoulidis, A. P.; He, J.; Malliakas, C. D.; Kanatzidis, M. G. *Adv. Mater.* **2011**, *23*, 4857.

(29) Rouquerol, F.; Rouquerol, J.; Sing, K. S. W. *Adsorption by Powders and Porous Solids: Principles, Methodology, and Applications*; Academic Press: San Diego, CA, 1999.

(30) Lopez, R. H.; Vidales, A. M.; Zgrablich, G. *Langmuir* **2000**, *16*, 6999.

(31) Janz, G. J.; Coutts, J. W.; Downey, J. R.; Roduner, E. *Inorg. Chem.* **1976**, *15*, 1755.

(32) Chang, C. H.; Chan, S. S. *J. Catal.* **1981**, *72*, 139.

(33) Janz, G. J.; Downey, J. R.; Roduner, E.; Wasilczyk, G. J.; Coutts, J. W.; Eluard, A. *Inorg. Chem.* **1976**, *15*, 1759.

(34) Kim, K. W.; Kanatzidis, M. G. *Inorg. Chem.* **1993**, *32*, 4161.

(35) Liang, B. Y.; Wang, X. F.; Andrews, L. *J. Phys. Chem. A* **2009**, *113*, 3336.